Growth Kinetics of One-Dimensional $KNbO_3$ Nanostructures by Hydrothermal Processing Routes

E. Vasco,*,† A. Magrez,‡ L. Forró,‡ and N. Setter†

Laboratoire de Céramique, Institut des Matériaux, and Laboratoire des Nanostructures et des Nouveaux Matériaux Electroniques, Institut de Physique de la Matière Complexe, Ecole Polytechnique Fédérale de Lausanne, CH-1015 Lausanne−EPFL, Switzerland

Received: March 21, 2005; In Final Form: June 7, 2005

The growth kinetics of one-dimensional single-crystalline $KNbO_3$ nanostructures (nanowires and nanofingers, the latter understood as defective nanowires) prepared by hydrothermal processing routes has been theoretically studied. A model taking into account the cube-based morphology of the nanostructures, their defects as the KOH proportion in the starting solution increases, and the partial depletion of species in the solution at the kink regions is proposed. Such a model allows the morphological evolution of the nanostructures to be successfully reproduced, shedding light on the origin of their highly anisotropic growth.

The development of a novel generation of nanoelectromechanical systems (NEMS) based on nanoscalable reliable components represents a technological challenge that captures the interest and creativity of the scientific community. In particular, preliminary progress recently achieved on preparing one-dimensional (1D) nanostructures (i.e., nanorods, nanowires, and nanotubes) of piezoelectric oxides[1−5] acts as a springboard to conceive futurist devices, for example, in the field of the nanorobotics.[6] However, major drawbacks (such as poor reproducibility) remain yet to be overcome before a high-performance device can be implemented. In this context, the control of the component shapes at the nanometer scale and the shape-dependent properties plays a crucial role in this technological crusade.[6] Such a control implies a precise understanding of the atomic mechanisms operating during the growth of anisotropic nanostructures, because the competition between mechanisms tuned through the growth parameters can be used as a morphology design tool.

$KNbO_3$ (KN hereafter) is a perovskite oxide with a wide spectrum of applications due to its attractive acoustooptic, electrooptic, nonlinear optical, and piezoelectric properties. Among such applications are stressed, for example, its use as (i) a frequency doubling and mixing material, (ii) a lead-free and biocompatible transductor with tunable piezoelectric response via Na-, Li-, and/or Ta doping,[7] and (iii) an optical waveguide and holographic storage medium. At moderate pressures,[8] KN undergoes several structural phase transitions, from cubic to tetragonal at 435 °C and then to orthorhombic and rhombohedral at 225 and −10 °C, respectively. KN has matured as a promising candidate for NEMS implementation since very recent studies[5,9] report its preparation by hydrothermal processing routes of samples (i.e., powders) 100% composed of uniform high-quality KN nanowires. Such single-crystalline nanowires (with carbon nanotube-like morphological qualities) exhibit aspect ratios (∼length-to-width ratio) as high as 100 and an average width of 60 nm. The so-prepared samples constitute a step ahead toward the mass production of 1D piezoelectric nanostructures. Within this framework, our work intends to shed light on the underlying mechanisms governing the anisotropic growth of these nanostructures and their interrelationships with the deposition parameters as a starting point for the future engineering of nanoscale functional oxides. This work complements preliminary studies[4,9,10] focused on the formation of supercritical-sized (as defined below) stoichiometric cubes, seeds for the spontaneous nucleation of nanostructures from chemical reactions occurring via dissolution−precipitation processes[10] within the supersaturated bath, as well as on the formation of the incipient nanowires.[4,9] It deserves to be mentioned that the origin of the highly anisotropic growth of 1D nanostructures of oxides (not only KN) with pseudocubic unit cells from solutions remains yet to be elucidated.

Reference 9 reports the existence of a small composition window of the starting solution for the preparation of high-quality single-crystalline nanowires. As the dissolved KOH amount increases moving away from optimal values (i.e., m_{KOH} becomes higher than 40% of solution net weight, wt %), for the Nb_2O_5 composition regime where highly anisotropic nanostructures are formed ($m_{Nb_2O_5} < 0.5$ wt %), the proportion of nanofingers (i.e., nanowires with nonuniform widths) in the population of 1D nanostructures increases. The nanofingers can be understood as defective nanowires as discussed below. A detailed inspection of nanofinger morphology as shown in Figure 1 reveals the following: (i) The nanofingers are made up by slightly distorted cubes (with aspect ratios $\sim 1.05 \pm 0.10$), which are uniaxially attached to each other along [011] KN.[11] (ii) The cube size (r) decreases in a stepped way with random step heights toward the nanofinger tip. These findings suggest that: (1) Cubes constitute the nanofinger/nanowire building blocks. (2) The previous cubes act as substrates or base surfaces for the nucleation and epitaxial growth of the next cubes. (3) The nucleation of a new cube takes place only on a substrate cube larger than a certain critical size (r_c), which is probably determined by the cube superficial tension. The latter suggestion would explain the nanofinger morphology as the result of a

* Author to whom correspondence should be addressed. Present address: Instituto de Ciencia de Materiales de Madrid, Cantoblanco, 28049 Madrid, Spain. E-mail: enrique.vasco@icmm.csic.es.

† Laboratoire de Céramique,Institut des Matériaux.

‡ Laboratoire des Nanostructures et des Nouveaux Matériaux Electroniques, Institut de Physique de la Matière Complexe.

10.1021/jp051454r CCC: $30.25
Published on Web 07/12/2005

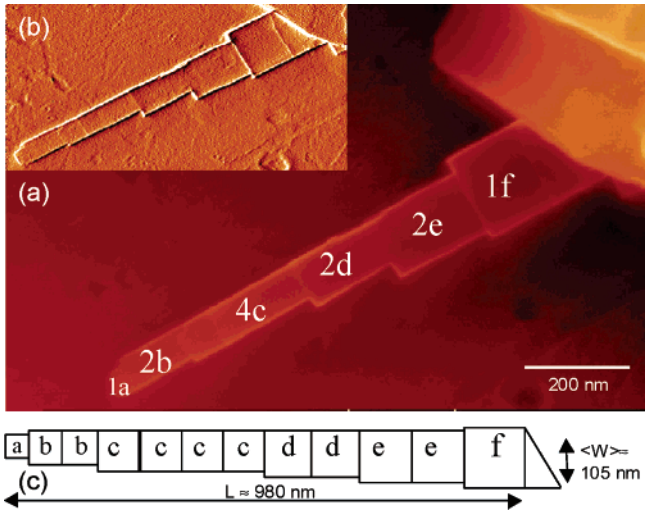

Figure 1. (a) Morphology of a nanofinger grown for 5 days by the hydrothermal route at 200 °C from a 44.4 wt % KOH + 0.4 wt % Nb_2O_5 + 55.2 wt % H_2O solution (SEM images). (b) Derivative of the image shown in part a where the cube-based nanofinger morphology is better displayed. (c) Sketch of the cube-based nanofinger morphology.

cumulative delay of growth times of successive cubes. On the basis of these suggestions, an analytical model to describe the morphological evolution of nanofingers (including the defect-free case, i.e., nanowires) is developed.

In the model, we assume that the nanofingers grow from a supersaturated solution with a uniform concentration ($\theta(\vec{\mathbf{r}},t) = \theta_0$) of constituent species, which acts as an infinite mass source[12] (i.e., the growth takes place far from the depletion regime of net concentration). The drain of the dissolved species by the nanofinger faces is locally compensated for by the species diffusion within the hydrothermal solution, which is characterized by a temperature- and pressure-dependent diffusion coefficient λ^2. Here, the diffusion coefficient has been considered high enough so that the width of the near-face region, where a concentration gradient exists on the basis of considering $\theta(\vec{\mathbf{r}},t) = 0$ on the capturing faces, is smaller than λ. Thus, if a cube face, with an area of r_1^2, captures $\sim r_1^2\lambda\theta_0$ particle/s by assuming a unitary sticking coefficient, the so-gained crystalline volume increases as

$$\frac{\partial V_1}{\partial t} = (r_0^{\,2} - r_1^{\,2})\lambda\theta_0\Omega + 4r_1^{\,2}\lambda\theta_0\Omega\varphi(t) + r_1^{\,2}\lambda\theta_0\Omega f(r_c - r_1) = 3r_1^{\,2}\frac{\partial r_1}{\partial t} \quad (1)$$

where Ω is the volume of captured particles, $\varphi(t)$ is a function ranging between 0 and 1 that accounts for the partial overlap of the capture regions of the base surface and the cube lateral faces, as shown in Figure 2a, the subscript index corresponds to the cube sequence number, and $f(y)$ is defined as $f(y) = 1$ for $y > 0$ and $f(y) = 0$ otherwise. Equation 1 is comprised by three contributions to the cube growth (Figure 2a): (I) the mass capture by the base surface followed by surface diffusion, which is assumed to be instantaneous (first term in eq 1), (II) the mass capture by the lateral cube faces (second term), and (III) the mass capture by the frontal cube face (third term). $f(y)$ takes into account that the frontal face of a supercritical-sized cube becomes the base surface for a new cube. The captured mass is redistributed through the cube surface (i.e., free surfaces and interfaces) to keep the aspect ratio of the building blocks constant, as given by the second equality in eq 1 that assumes a cube aspect ratio of 1.

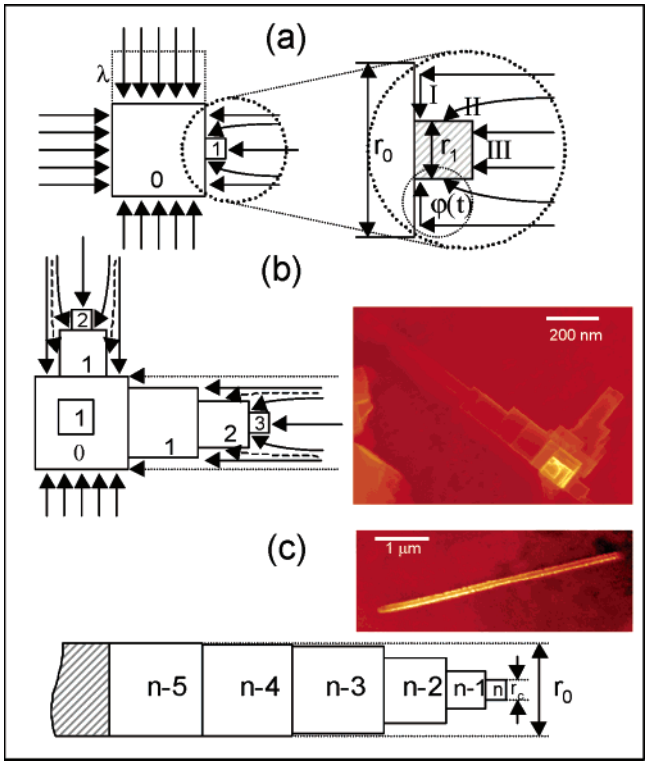

Figure 2. Sketch showing different stages of the nanofinger/nanowire growth kinetics. The insets in part b and c show several nanofingers growing from a single initial cube and an isolated nanostructure with uniform width (i.e., nanowire), respectively.

When eq 1 is generalized to any cube comprised within the sequence of m cubes that shapes the nanofingers (Figures 2b and 2c), the rate equation describing the nanofinger growth can be written as

$$\frac{\partial r_n}{\partial(t - t_n)} = \frac{\phi}{3}\left\{\left[\left(\frac{r_{n-1}}{r_n}\right)^2 - 1\right] + 4\varphi(t) + f(r_c - r_n)\right\} \quad (2)$$

where $\phi = \lambda\theta_0\Omega$ and t_n is defined as $r_{n-1}(t_n) = r_c$. Equation 2 cannot be used to describe the cube nucleation regime since $\partial r_n/\partial t \rightarrow \infty$ when $r_n \rightarrow 0$ lacks of physical meaning. So, the nucleation and early growth stages should be addressed by replacing the first bracketed term in eq 2 (i.e., the base surface contribution to the cube growth) with $r_{n-1}(\phi r_{n-1}t)^{-2/3}$ for $r_{n-1} \gg r_n$. The nucleation of the successive cubes on the surfaces of the previous ones, which takes place probably from surface defects, becomes spontaneous (with negative Gibbs free energy) from the supersaturated bath in hydrothermal conditions and gives rise to an homoepitaxial growth as reported in ref 9.

The solution of eq 2 requires computing the function $\varphi(t)$ via solution of the diffusion equation (Fick's second law) in kink areas enclosed by cube lateral faces and the base surface, which act as drain boundaries

$$\frac{\partial\theta}{\partial t} = \frac{\partial}{\partial\vec{\mathbf{r}}}\left(\lambda^2\frac{\partial}{\partial\vec{\mathbf{r}}}\theta(\vec{\mathbf{r}},t)\right) - \vec{\mathbf{r}}_s\lambda\theta(\vec{\mathbf{r}} \rightarrow \vec{\mathbf{r}}_s,t) - f(t - t_n)\vec{\mathbf{r}}_f(t)\lambda\theta(\vec{\mathbf{r}} \rightarrow \vec{\mathbf{r}}_f,t) \quad (3)$$

The above equation is solved in a $x-y$ kink plane (with y along the nanostructure axis, as shown in Figure 3a) away from the edges of the involved cubes using $\theta(\vec{\mathbf{r}},t = 0) = 1$ ($\theta(\vec{\mathbf{r}} = \vec{\mathbf{r}}_s$ or $\vec{\mathbf{r}}_f,t) = 0$ and $\theta(\vec{\mathbf{r}} \rightarrow \infty,t) = 1$) as initial (boundary) conditions. $\vec{\mathbf{r}}_s \in \{(l \ldots \infty, 0)\}$ and $\vec{\mathbf{r}}_f \in \{(l, 0 \ldots 2l)\}$ identify the positions on the base surface and cube lateral faces, respectively, $l =$

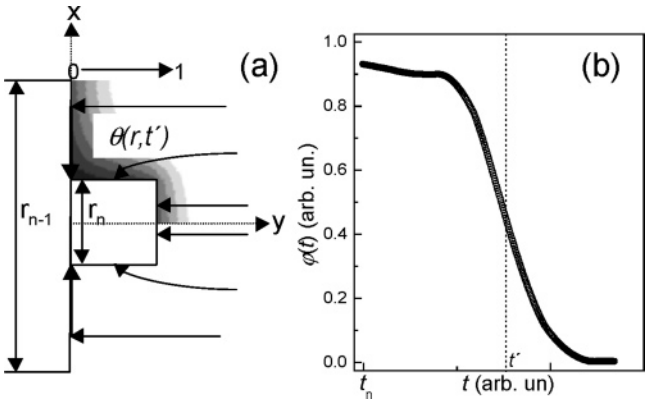

Figure 3. $\varphi(t)$ calculated from numerical solution of eq 3, $\theta(\vec{\mathbf{r}},t)$, which is shown in the form of contour plot in part a for an arbitrary time, t'. The contour plot is scaled in arbitrary units according to the boundary conditions: $\theta(\vec{\mathbf{r}} \rightarrow \infty,t) = 1$ and $\theta(\vec{\mathbf{r}} \rightarrow$ nanofinger surface,$t) = 0$.

$^1/_2\sqrt[3]{\Omega\int[\theta(\vec{\mathbf{r}},t_n)-\theta(\vec{\mathbf{r}},t)]\partial\vec{\mathbf{r}}^2}$ being the half lateral size of the growing cube. The so-defined boundary conditions take into consideration the cube coarsening with the mass capture for $t > t_n$ accounting for the forward movements of the cube faces. In this calculation, the function $\varphi(t)$ represents the time-dependent ratio per surface unit of the mass captured by the lateral cube faces to the mass captured by the base surface at kink regions,[13] neglecting the capture by the frontal face.

Figure 3a shows the numeric solution of eq 3 for a generic $t > t_n$. The capture area of the lateral faces runs parallel to the base surface comprising mostly the region of the composition gradient previously created in front of the base surface (Figure 3a). $\varphi(t)$ collects complementary influences of several effects operating simultaneously: (i) For the mass capture by the lateral faces of a growing cube, the capture rate increases as cube size increases. (ii) Such a mass capture occurs within the region moderately depleted by the base surface capture. It gives rise to an anticipated depletion of the solution concentration at the kinks, which are the less accessible regions of the capturing area. (iii) The depletion phenomenon is partially compensated for by the forward movements of cube faces. Thus, $\varphi(t)$ as plotted in Figure 3b reveals that the contribution of the capture by the lateral faces (contribution II in Figure 2a) to the cube growth decreases progressively, which would hinder the nucleation of new cubes on the lateral faces. This prediction is in agreement with our experimental evidence that points to the nonexistence of branches in the wide set of nanofingers investigated. Hence, the highly anisotropic growth of nanostructures, such as nanofingers and/or nanowires, in a hydrostatic (∼isotropic) medium from pseudo-cubic building blocks would be the result of a depletion phenomenon of the solution concentration at the nanostructure lateral faces.

The competition between the three contributions collected in eqs 1 and 2 gives rise to three growth regimes of the stacked cubes. At early growth time $t_n \leq t < t_{n+1}$, the cube size increases with a quasi-linear dependence of t exhibiting a coarsening rate of $\sim 5\phi/3$. This first regime is governed by contributions II (capture by the lateral faces) and III (capture by the frontal face). For $t \approx t_{n+1} = 3r_c/5\phi + t_n$, a new cube nucleates on the frontal face; consequently, contribution III vanishes, causing a decrease in the coarsening rate down to $\sim 4\phi/3$. At longer growth times ($t > t'$ so that $\varphi(t') = 0.5$), as the size of the coarsening cube approaches that of the base cube ($r_n \rightarrow r_{n-1}$, for practical purposes $r_n > r_{n-1}/\sqrt{5}$), a saturation regime controlled by contribution I (capture by the base surface) is reached. In this third regime, the cube size tends asymptotically to the size of the initial cube ($r_n \rightarrow r_0$), giving rise to 1D nanostructures with uniform widths (e.g., nanowires, inset of Figure 2c). Unlike the growth kinetics of the successive cubes, the coarsening of the initial cube (i.e., $r_0 = r_0(t)$) is controlled by the mass capture by the cube faces free of nanofingers. Hence, as experimentally observed (Figure 2b), different faces of the initial cube act as base surfaces for the growth of several nanofingers. The number of nanofingers developed per face depends on the r_0/λ ratio. The linear regimes determine the stepped morphology of the growth front of the nanofingers, predicting the existence of a regular sequence of $5(r_0 - r_c)/4r_c + 2$ cubes with decreasing sizes. The sizes of these cubes scale down in a linear way toward the nanofinger tip. The proposed model (eq 2) reproduces successfully the early stages of the nanofinger/nanowire growth as shown in the inset of Figure 4a. To fit the data to the model, r_c is taken from averaging the sizes of the two smallest cubes (typically $r_c \approx 50-60$ nm), r_0 is inferred as the saturation size (typically r_0 exhibits a large dispersion of values, $r_0 = 150-350$ nm), and the time axis is plotted in nucleation time units of a new cube (i.e., $\Delta t_n = t_{n+1} - t_n = 3r_c/5\phi =$ a constant that corresponds to a time unit), referred to the time of origin of the nanofinger ($t_1 = 0$).

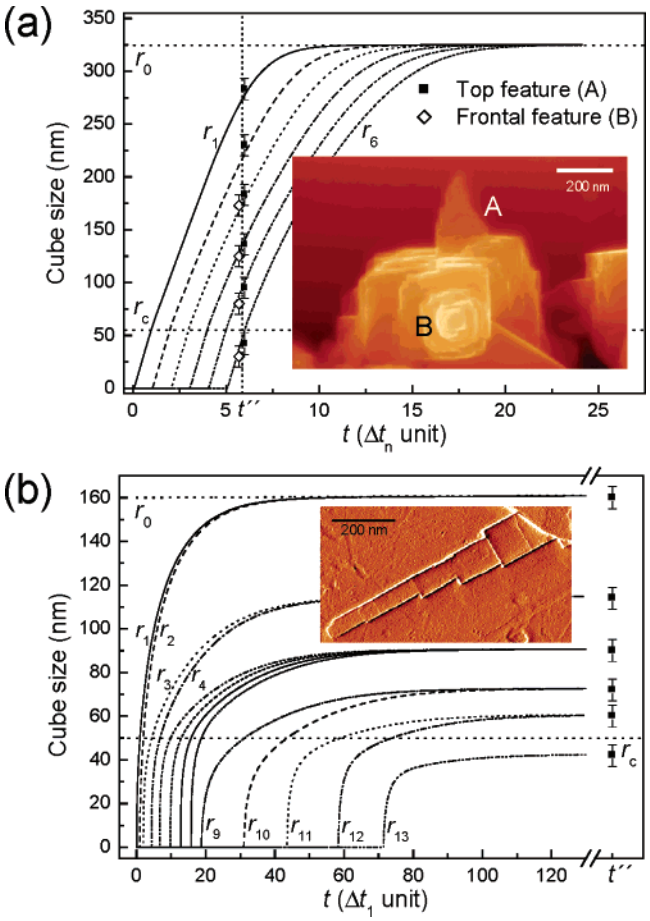

Figure 4. Nanofinger morphologies modeled from (a) eq 2 and (b) eq 4. The curves are the numerical solutions; the symbols correspond to experimental sizes measured in typical nanofingers (SEM images shown in the figure insets) by assuming a cube-based morphology and arbitrary growth times (t''). The dotted lines denote r_0 and r_c used in the simulation. The set of Δ_n values (for $0 \leq n < 13$) used in part b was $\Delta_n = \{1, 1, 0.71, 1, 0.79, 1, 1, 1, 0.80, 1, 0.83, 1, 0.7\}$.

However, this model does not reproduce the morphology of 1D nanostructures with nonuniform widths such as the nanofinger shown in Figure 1. These nonuniform widths have been previously related to the presence of defects in the bulk of the

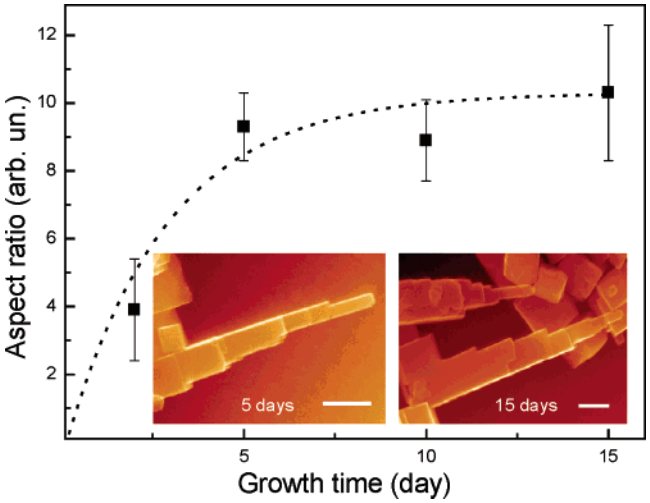

Figure 5. Evolution of nanofinger aspect ratio. SEM Images of typical nanowires grown by the hydrothermal route at 200 °C for 5 and 15 days from a 44.4 wt % KOH + 0.4 wt % Nb_2O_5 + 55.2 wt % H_2O solution. Scale bar corresponds to 200 nm.

1D inorganic nanostructure.[14] Such defects would block a fraction of the base surface, shrinking the effective nucleation/coarsening area for successive cubes. The study of a wide set of nanofingers reveals that the nanostructure width decreases stochastically in a stepped way. Since slightly distorted cubes constitute the nanofinger building blocks, as commented above, the step height and step separation correspond to the size difference between consecutive cubes ($r_n - r_{n+1} = r_n(1 - \Delta_n) \geq 0$, with Δ_n taking random values ranging between 0 and 1) and $\sim m r_n$ (with m being a random integer), respectively. To consider the influence of the defects on the growth kinetics of the nanofingers, the rate equation in eq 2 is modified as

$$\frac{\partial r_n}{\partial(t - t_n)} = \frac{\phi}{3}\left\{\left[\left(\frac{r_{n-1}\Delta_{n-1}}{r_n}\right)^2 - 1\right] + 4\varphi(t) + f(r_c - r_n)\right\} \quad (4)$$

where $\Delta_{n-1}{}^2$ corresponds to the fraction not blocked by defects of the base surface $r_{n-1}{}^2$. The so-reformulated rate equation describes fairly the growth of nanowires (nanofingers in Figure 4b) from the condition $\Delta_n = 1$ for every n ($\Delta_n < 1$ for some n). Since Δt_n increases with n (i.e., $\Delta t_n \neq$ constant) under the nanofinger growth condition as $\Pi_i^p \Delta_i \rightarrow r_c/r_0$ (p being the number of stacked cubes), the time axis in Figure 4b is normalized with respect to Δt_1 rather than to Δt_n. In addition, eq 4 predicts the existence of a saturation value for the nanofinger aspect ratios once the inequality $\Pi_i^p \Delta_i \leq r_c/r_0$ is satisfied. The saturation of the aspect ratios to a value of $\sim$10 has been experimentally detected (as shown in Figure 5) in nanofingers grown for longer than 5 days in hydrothermal baths from a 44.4 wt % KOH solution ($m_{Nb_2O_5} = 0.4$ wt %). The average aspect ratios and error bars displayed in Figure 5 have been estimated over large populations (<50) of 1D nanostructures. The moderate increase of the width of the aspect ratio distribution (estimated as the error bars) with the growth time indicates all the nanostructures are formed during the first 5 days, so that a relatively narrow nanofinger shape distribution is found for longer times. It suggests that for such times the mass capture by the coarsening nanofingers prevails over the nucleation of new nanostructures. Once the nanofinger coarsening is blocked by the defect accumulation, the growth can only proceed via the coarsening of the initial cube, which is the slowest process involved in the growth kinetics of the nanofingers.

The nature of the defects blocking the coarsening of the successive cubes remains yet to be elucidated. Bright field measurements by transmission electron microscopy (TEM) do not provide conclusive results that allow unambiguous connection of the width steps with structural defects in the bulk of the nanofingers, such as dislocations or grooves. The increase of the proportion of nanofingers in the population of 1D nanostructures with the increasing concentration of KOH in the solution suggests that such defects could have a stoichiometric nature, e.g., composition gradients, Nb-depleted regions, etc. In this sense, further studies of nanofingers by local techniques such as high-resolution TEM and nano-probe chemical analysis are required.

In conclusion, the growth kinetics of 1D KN nanostructures (nanowires and nanofingers, the latter understood as defective nanowires) prepared by hydrothermal routes has been studied and modeled successfully. The proposed model provides a plausible explanation to address the paradigmatic origin of highly anisotropic oxide nanostructures grown from an isotropic medium (as the hydrothermal solution) using slightly distorted cubes as building blocks.

References and Notes

(1) Urban, J. J.; Yun, W. S.; Gu, Q.; Park, H. *J. Am. Chem. Soc.* **2002**, *124*, 1186−1187.
(2) Yun, W. S.; Urban, J. J.; Gu, Q.; Park, H. *Nano Lett.* **2002**, *2*, 447.
(3) Mao, Y. B.; Banerjee, S.; Wong, S. S. *J. Am. Chem. Soc.* **2003**, *125*, 15718−15719.
(4) Liu, J. F.; Li, X. L.; Li, Y. D. *J. Cryst. Growth* **2003**, *247*, 419−424.
(5) Suyal, G.; Colla, E.; Gysel, R.; Cantoni, M.; Setter, N. *Nano Lett.* **2004**, *4*, 1339−1342.
(6) Requicha, A. A. G. *Proc. IEEE* **2003**, *91*, 1922−1933.
(7) Saito, Y.; Takao, H.; Tani, T.; Nonoyama, T.; Takatori, K.; Homma, T.; Nagaya, T.; Nakamura, M. *Nature* **2004**, *432*, 84−87.
(8) Pruzan, P.; Gourdain, D.; Chervin, J. C. *High Pressure Res.* **2002**, *22*, 243−249.
(9) Magrez, A.; Vasco, E.; Seo, J.-W.; Dieker, C.; Setter, N.; Forró, L. Synthesis of Single-Crystalline $KNbO_3$ Nanowires. *Chem. Commun.*, submitted for publication.
(10) Hayashi, H.; Hakuta, Y.; Kurata Y. *J. Mater. Chem.* **2004**, *14*, 2046−2051.
(11) Indexed referring to the *Amm*2 orthorhombic KN unit cell.
(12) It is assumed that under hydrothermal conditions the Brownian motion and the circulation rate of the dissolved species are enhanced.
(13) The $\theta(r,t)$ calculation was performed within a kink area of $r_{n-1}/2 \times r_{n-1}/2$.
(14) Tang, C. C.; Bando, Y.; Golberg, D. *J. Solid State Chem.* **2004**, *177*, 2670−2674.